

A Liquid-Metal–Elastomer Nanocomposite for Stretchable Dielectric Materials

Chengfeng Pan, Eric J. Markvicka, Mohammad H. Malakooti, Jiajun Yan, Leiming Hu, Krzysztof Matyjaszewski, and Carmel Majidi*


Stretchable high-dielectric-constant materials are crucial for electronic applications in emerging domains such as wearable computing and soft robotics. While previous efforts have shown promising materials architectures in the form of dielectric nano-/microinclusions embedded in stretchable matrices, the limited mechanical compliance of these materials significantly limits their practical application as soft energy-harvesting/storage transducers and actuators. Here, a class of liquid metal (LM)–elastomer nanocomposites is presented with elastic and dielectric properties that make them uniquely suited for applications in soft-matter engineering. In particular, the role of droplet size is examined and it is found that embedding an elastomer with a poly-disperse distribution of nanoscale LM inclusions can enhance its electrical permittivity without significantly degrading its elastic compliance, stretchability, or dielectric breakdown strength. In contrast, elastomers embedded with microscale droplets exhibit similar improvements in permittivity but a dramatic reduction in breakdown strength. The unique enabling properties and practicality of LM–elastomer nanocomposites for use in soft machines and electronics is demonstrated through enhancements in performance of a dielectric elastomer actuator and energy-harvesting transducer.

strategy for developing these soft material systems is to mix inorganic filler into a soft organic polymer, resulting in a composite that combines the mechanical properties of the polymer matrix with the electrical and thermal properties of the inorganic dispersion phase.^[23–31] However, a limitation of this approach is that the high filler concentrations required to enhance electrical or thermal properties will often lead to a degradation in the mechanical properties of the polymer and cause the composite to become more stiff and less elastic.^[32,33] For instance, Gallone et al.^[32] enhance the dielectric constant of silicone elastomer by a factor of three (from 6.86 to 19.6) by filling the rubber with 30% by volume rigid ferroelectric powder. However, the addition of filler degrades the strain at break from 500% down to 200% and increases the elastic modulus from 62 to 135 kPa. One promising alternative is to replace the rigid fillers that are commonly used in soft polymer composites with droplets of liquid metal (LM). These LM-embedded elastomer (LMEE) composites uniquely combine the compliance and elasticity of soft silicone rubber with high dielectric constant,^[27,34] high thermal conductivity,^[28–31] and fracture toughness.^[35]

Soft materials capable of sensing^[1–5] actuation,^[6–8] and energy storage and harvesting^[9–13] represent key components for emerging applications in wearable electronics,^[14–17] soft robotics,^[4,18,19] and biocompatible soft devices.^[20–22] A common

droplets of liquid metal (LM). These LM-embedded elastomer (LMEE) composites uniquely combine the compliance and elasticity of soft silicone rubber with high dielectric constant,^[27,34] high thermal conductivity,^[28–31] and fracture toughness.^[35]

C. F. Pan, Dr. M. H. Malakooti
Integrated Soft Materials Lab
Carnegie Mellon University
Mechanical Engineering
Carnegie Mellon University
Pittsburgh, PA 15213, USA
Prof. E. J. Markvicka^[†]
Integrated Soft Materials Lab
Carnegie Mellon University
Robotics Institute
Carnegie Mellon University
Pittsburgh, PA 15213, USA

 The ORCID identification number(s) for the author(s) of this article can be found under <https://doi.org/10.1002/adma.201900663>.

^[†]Present address: Mechanical and Materials Engineering, University of Nebraska-Lincoln, Lincoln, NE 68588, USA

^[††]Present address: Materials Science Division, Lawrence Berkeley National Laboratory, Berkeley, CA 94720, USA

Dr. J. J. Yan,^[††] Prof. K. Matyjaszewski
Chemistry
Carnegie Mellon University
Pittsburgh, PA 15213, USA
L. M. Hu
Mechanical Engineering
Carnegie Mellon University
Pittsburgh, PA 15213, USA
Prof. C. Majidi
Integrated Soft Materials Lab
Carnegie Mellon University
Mechanical Engineering
Carnegie Mellon University
Robotics Institute
Carnegie Mellon University
Material Science and Engineering
Carnegie Mellon University
Pittsburgh, PA 15213, USA
E-mail: cmajidi@andrew.cmu.edu

DOI: 10.1002/adma.201900663

Some formulations of LMEE can also be engineered to be electrically conductive^[36,37] and function as wiring for stretchable digital circuits with electrically “self-healing” properties.^[38] When integrated into a soft robotic system, such materials can function as an artificial muscle tissue that manages heat generated by an embedded thermal actuator^[28] or an adaptive nervous tissue that reconfigures its network of electrically conductive pathways in response to mechanical damage.^[38]

Until now, LMEEs have been synthesized with polydisperse suspensions of micro-sized droplets (diameter $\approx 2\text{--}50\text{ }\mu\text{m}$) of eutectic gallium indium (EGaIn) (Table S1, Supporting Information). In contrast to rigid inorganic particles—e.g., silver powder, carbon nanotubes, barium titanate, and other metallic, carbon, or ceramic particles^[27,39]—these EGaIn droplets freely deform with the surrounding polymer and have limited influence on elastic compliance and strain limit. They enable LMEEs to behave like an “artificial dielectric” with a much higher electrical permittivity and electromechanical coupling coefficient than other dielectric elastomers with similar mechanical compliance. However, one key limitation of LMEEs is the reduced dielectric breakdown strength that arises from their heterogeneous microstructure (Section 2 and Tables S2 and S3 Supporting Information). For applications involving electro-mechanical actuation, electrostatic energy storage, energy harvesting, or high voltage electronics, it is necessary to re-engineer LMEEs so that they can exhibit enhanced electrical permittivity while preserving the breakdown strength of the polymer matrix. One approach is to replace the micro-sized droplets currently used in LMEEs with smaller submicrometer droplets since it is well known that smaller inclusions will reduce the intensity of internal charge and field concentrations that lead to electrical breakdown.^[40,41] For example, Roy et al. reported the increase in dielectric breakdown strength for the titanium dioxide-epoxy resin nanocomposite over microcomposite.^[41] In addition to the influence on dielectric breakdown strength, the size of fluidic LM filler may also affect the mechanical properties of LM-elastomer composites. Recently, Style et al. reported variations in the stiffness of silicone gel composites that scaled differently with ionic-liquid inclusions depending on whether the inclusions were nano- or micro-sized.^[42] Apart from their potentially transformative role in soft-matter engineering, LM-elastomer composites serve as a unique model material for understanding the interplay between the dielectric and mechanical properties that arise in soft multiphase material systems.

Here, we report a class of stretchable LM-elastomer nanocomposites (Figure 1a,b) and investigate the size effect of LM inclusions on the dielectric and mechanical properties of these composites. Different synthesis methods are developed to create composites that are embedded with EGaIn inclusions with diameters on the order of 100 nm, 1 μm , and 10 μm (Figure 1c). The dielectric breakdown strength (E_b) and mechanical strain at break of these composites with different volume fraction (ϕ) of LM are presented in Figure 1d. As shown in the leftmost plot, LM-elastomer composites with the O(10 μm)-sized inclusions exhibit a significant degradation in dielectric breakdown strength and strain limit when LM is added, even for filler concentrations as low as 10 vol%. In contrast, composites with smaller LM inclusions (O(1 μm) and O(100 nm)) maintain their mechanical strain limit (i.e., stretchability) over

a relatively wide range of filler concentrations and the degradation in E_b is significantly more modest. Details of the mechanical and dielectric properties of the LM-elastomer composites are presented below.

We first evaluate breakdown strength of LM-elastomer composites as a function of ϕ for LM inclusions with different LM droplet sizes, i.e., diameter of O(10 μm), O(1 μm), and O(100 nm) (Figure 2a, Figure S2, Supporting Information). For the results presented in Figure 2a–c, we used poly(dimethylsiloxane) (PDMS)-Sylgard 184 as the matrix polymer for all samples. For composites with a filler diameter of O(10 μm), E_b decreases dramatically with the addition of EGaIn droplets, i.e., from 135 to 2 kV mm^{−1} with a filler volumetric fraction of $\phi = 10\%$. We attribute this degradation to internal electric field concentrations that arise from having a highly polydisperse, heterogeneous dispersion (Figure S3a, Supporting Information) with average droplet diameters ($\approx 38\text{ }\mu\text{m}$, Figure S4a, Supporting Information) within an order of magnitude of the composite film thickness ($\approx 120\text{ }\mu\text{m}$). Such a coarse microstructure results in the presence of poorly insulated pathways between the two surfaces of the film (Figure S3b; see also discussion in Section 2, Supporting Information). Because breakdown in these microcomposites is driven by the existence of at least one poorly insulated pathway (rather than scaling with the number of such pathways), the degradation in E_b tends to saturate with increasing EGaIn volumetric fraction for $\phi = 10\%$ to 40%.

In contrast, LM-elastomer nanocomposites, which have inclusions that are small compared to the gross dimensions of the film, will exhibit a less dramatic monotonic decrease in E_b with increasing ϕ (Figure 2a). We plot E_b versus ϕ (Figure 2a inset) and find that, at low loading fraction ($\phi = 5\%$), composites with O(100 nm) filler have a slightly greater breakdown strength ($E_b = 122\text{ kV mm}^{-1}$) than for samples with larger O(1 μm) filler ($E_b = 111\text{ kV mm}^{-1}$). A plausible explanation is that, at low volume fractions of LM, the interparticle distance between adjacent LM inclusions is too large to cause significant interfacial electric field concentrations. Composites with smaller size filler will then be less susceptible to partial discharge, electric treeing, or the propagation of regions of material degradation from internal electric breakdown.^[43] Moreover, the inclusions in the O(100 nm) nanocomposites will have smaller localized field concentrations on account of their smaller dimensions.^[43] Interestingly, as ϕ increases, the nanocomposites show a more rapid decline in E_b than composites with O(1 μm) inclusions. We attribute this to the larger number of droplets in the O(100 nm) composite, which results in closer proximity between adjacent droplets and more significant interparticle interactions. Another possible reason for this difference is that the O(1 μm) composites have higher polydispersity of EGaIn droplets (Figure S4b,c, Supporting Information), with the nanoscale EGaIn droplets acting as interstitials between microscale EGaIn droplets. This allows for a “best of both worlds” scenario in which the larger droplets allow for greater average spacing and the smaller droplets correspond to smaller local field concentrations.^[43]

To further examine the dielectric properties of LM-elastomer material systems, we perform measurements to establish their electrical polarizability and charge storage capacity. We do this by measuring the effective relative permittivity (ϵ_r) and

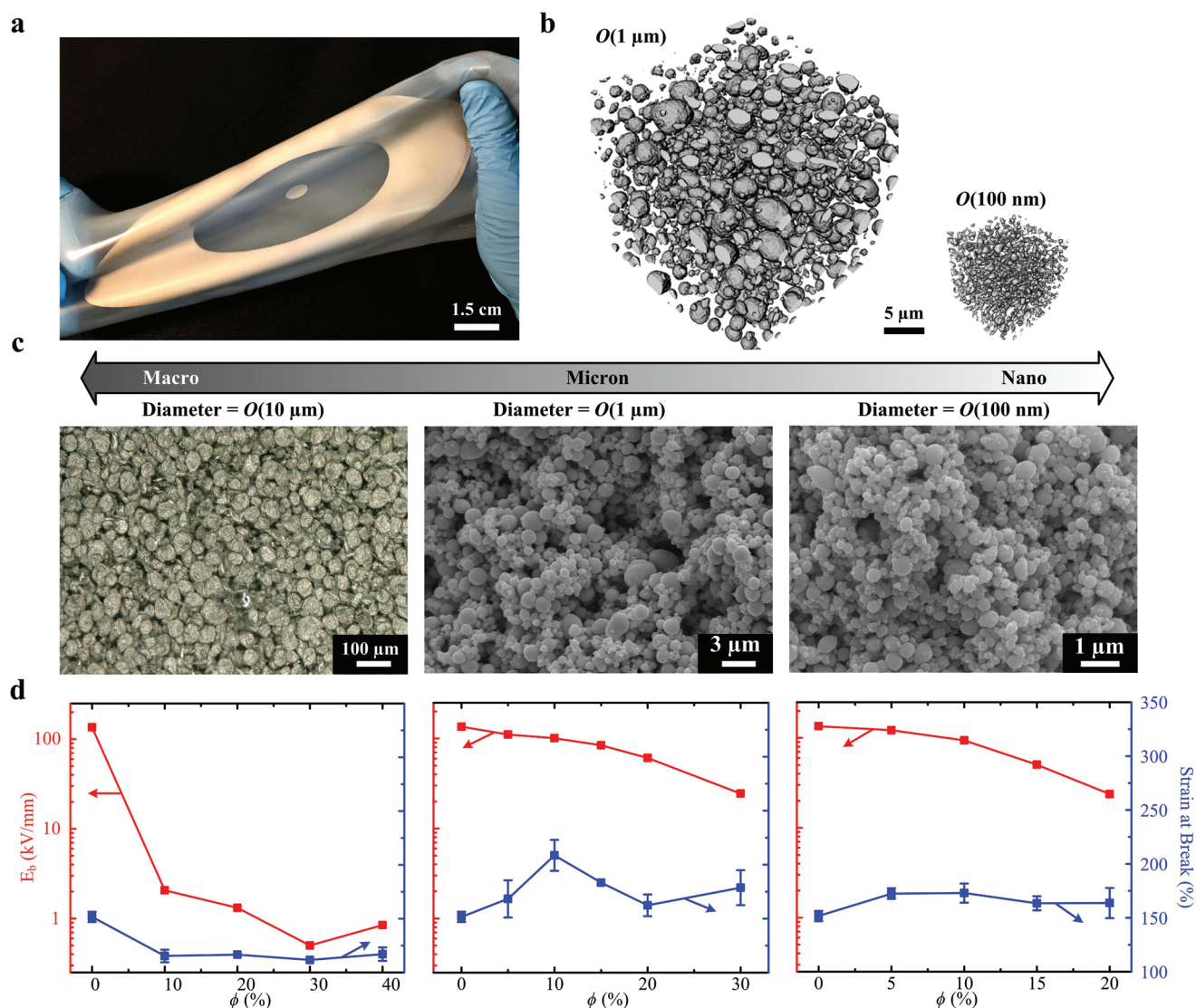


Figure 1. LM-elastomer composites. a) Image of stretched LM-elastomer nanocomposite (silver; annular shape) on a silicone elastomer carrier film (semitransparent). b) Nanoscale X-ray computed tomography (Nano-CT) scan showing the 3D microstructure indicating homogeneous dispersion of LM droplets in matrix for both composites with LM diameter of $O(1 \mu\text{m})$ —left and $O(100 \text{ nm})$ —right on the same scale. c) Microscopic images of LM droplets with diameter of $O(10 \mu\text{m})$ —left, $O(1 \mu\text{m})$ —middle, and $O(100 \text{ nm})$ —right. The left image presents the top view of a composite with an elastomer matrix and $O(10 \mu\text{m})$ droplets made by shear mixing bulk LM with elastomer. d) Weibull dielectric breakdown strength and mechanical strain at break for LM-elastomer composites with corresponding filler diameters of $O(10 \mu\text{m})$ —left, $O(1 \mu\text{m})$ —middle, and $O(100 \text{ nm})$ —right.

dissipation factor (D) as a function of ϕ for the three types of LM-elastomer composites in order to investigate the influence of filler size (Figure 2b,c). These measurements are performed at a frequency of 1 kHz and a potential bias of 1 V. Figure 2b shows that ϵ_r increases monotonically and nonlinearly as ϕ increases. To see how this observation compares with trends in effective medium theory (EMT), we fit the experimental data with theoretical curves obtained using a model by Nan et al.^[44] (dashed line)

$$\epsilon_{rc} = \epsilon_{rm} \frac{1 - 2\alpha + 2\phi(1 + \alpha)}{1 - 2\alpha - \phi(1 + \alpha)} \quad (1)$$

where ϵ_{rc} and ϵ_{rm} are the dielectric constant of the composite and the matrix, respectively. The parameter α is a dimensionless value that is associated with the diameter of the droplets, i.e., smaller inclusions correspond to a larger α . The fittings suggest that the measured influence of ϕ on ϵ_r is in good agreement with EMT for reasonable values of the interfacial factor α . The electrical dissipation factor, also called the dielectric loss tangent, is defined as the ratio of the dielectric power loss to the reactive capacitance power during alternating current (AC) oscillation. For the LM-polymer composites, D is measured to be small (<0.007) compared to other dielectric materials (Table S3, Supporting Information) and exhibits only modest

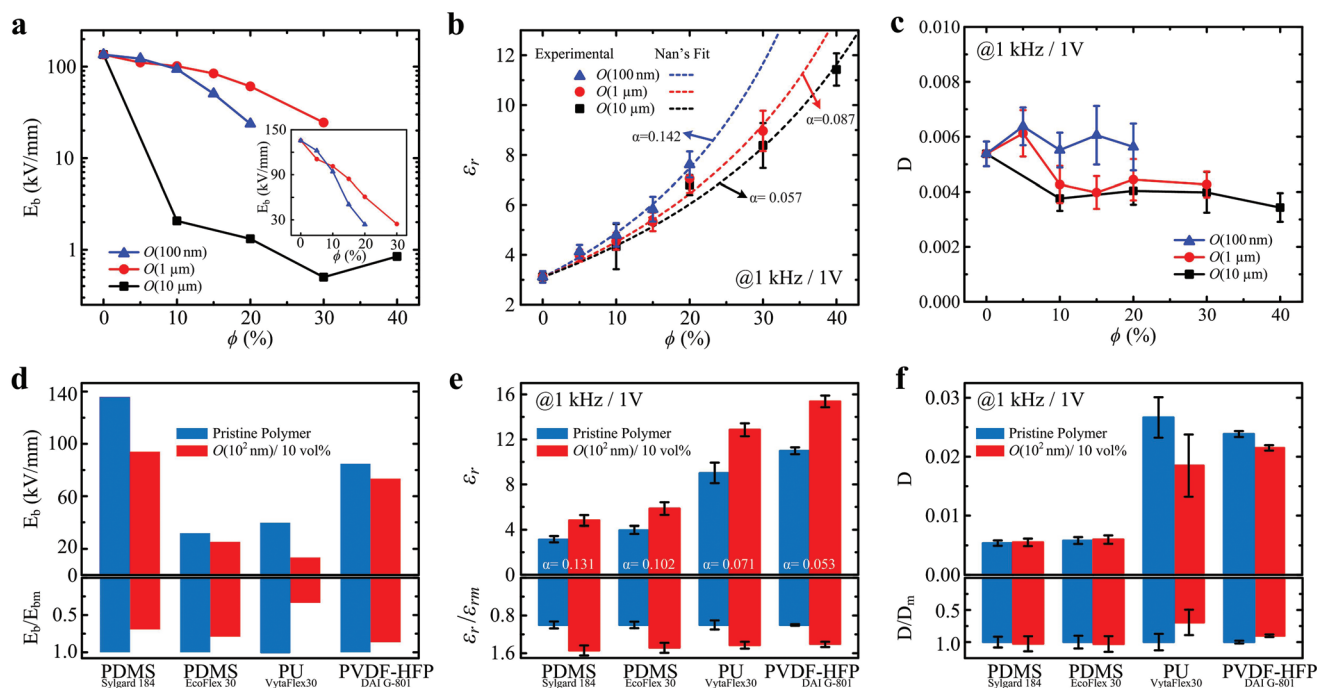


Figure 2. Dielectric properties of LM-elastomer composites. a–c) LM-PDMS (Sylgard 184) composites: a) Weibull breakdown strength as a function of LM filler content on a logarithmic scale. Inset: Weibull breakdown strength in linear scale b) Effective dielectric constant as a function of LM filler content. The dashed lines are the theoretical fit with an effective medium theory. c) Dissipation factor as a function of LM filler content. d–f) LM-elastomer nanocomposites: d) Weibull breakdown strength: absolute value—top, and normalized value—bottom. e) Effective dielectric constant, absolute value—top, and normalized value—bottom. f) Dissipation factor: absolute value—top and normalized value—bottom.

variation among the various samples. This low dissipation factor suggests the potential for reliable electrostatic energy storage with capacitors containing LM-elastomer micro- or nanocomposites as the dielectric. However, we should note that the $O(1\text{ }\mu\text{m})$ and $O(10\text{ }\mu\text{m})$ composite systems have a lower D than the $O(100\text{ nm})$ composites. We also investigate ϵ_r and D across the frequency range of 0.1 to 200 kHz at a potential bias of 1 V (see Figures S5 and S6, Supporting Information). The results show that LM-elastomer composites exhibit a uniform value for ϵ_r and has small value (<0.05) over whole frequency range (see detailed discussion in Section 2 in the Supporting Information).

We next select $O(100\text{ nm})$ EGaIn nanodroplets as filler to investigate how the choice of matrix polymer will influence the dielectric properties of LM-elastomer composites (see Figure S7, Supporting Information). In addition to Sylgard 184 PDMS, we synthesized nanocomposites using three other matrix materials: a softer silicone (EcoFlex 30), polyurethane (PU; Vytaflex 30), and poly(vinylidene fluoride-co-hexafluoropropylene) (PVDF-HFP; DAI G-801). In each case, we compared the dielectric properties of the unfilled polymer with LM-elastomer nanocomposites with $\phi = 10\%$ EGaIn volumetric fraction. As summarized in Figure 2d–f, similar trends of dielectric properties indicate that all polymer systems are compatible with the LM dispersion architecture. For example, the normalized enhancement of dielectric constant with LM inclusions is almost identical for all polymer systems ($\approx 50\%$ enhancement) (Figure 2e) and is consistent with the effective media theory (Nan's model^[44]). We also observe a small dissipation factor change (Figure 2f), suggesting that the nanocomposites can

separate or store electrical charge with minimum dielectric loss.

An exception to the observed trends is the LM-PU nanocomposite, which exhibits a dramatic reduction in dielectric breakdown strength (66% drop from 39.7 to 13.4 kV mm⁻¹) as well as a significant decrease in D (30% decrease from 0.026 to 0.018). One possible reason may be related to the intrinsic semicrystallinity of PU.^[45] The presence of LM inclusions potentially introduces disorder or defects within these semicrystalline domains that results in the decrease of the dielectric loss, i.e., a smaller dissipation factor. The larger mobility of electron and dipole moments within the PU chains^[46] caused by LM inclusions could be responsible for the dramatic degradation in breakdown strength for LM-PU nanocomposites. Although the precise reasons for the degraded performance remain to be fully understood, experimental measurements clearly suggest that polyurethane is a relatively poor choice as a matrix material for dielectric elastomer actuators, capacitive energy storage, or electromechanical energy harvesting.

In contrast to the PU-based composites, LM nanocomposites with a PVDF-HFP matrix appear to exhibit the best performance, i.e., the highest electric permittivity, enabled by spontaneously oriented carbon-fluorine dipoles within ferroelectric domains, and relatively limited reduction in breakdown strength due to the homogeneous disordering of the PVDF-HFP crystalline structures (see detailed discussion of LM-PU and LM-PVDF-HFP in Section 3 in the Supporting Information). The high dielectric constant and breakdown strength of PVDF-based composites is the main reason why these materials are popular as dielectrics. However, the low stretchability of

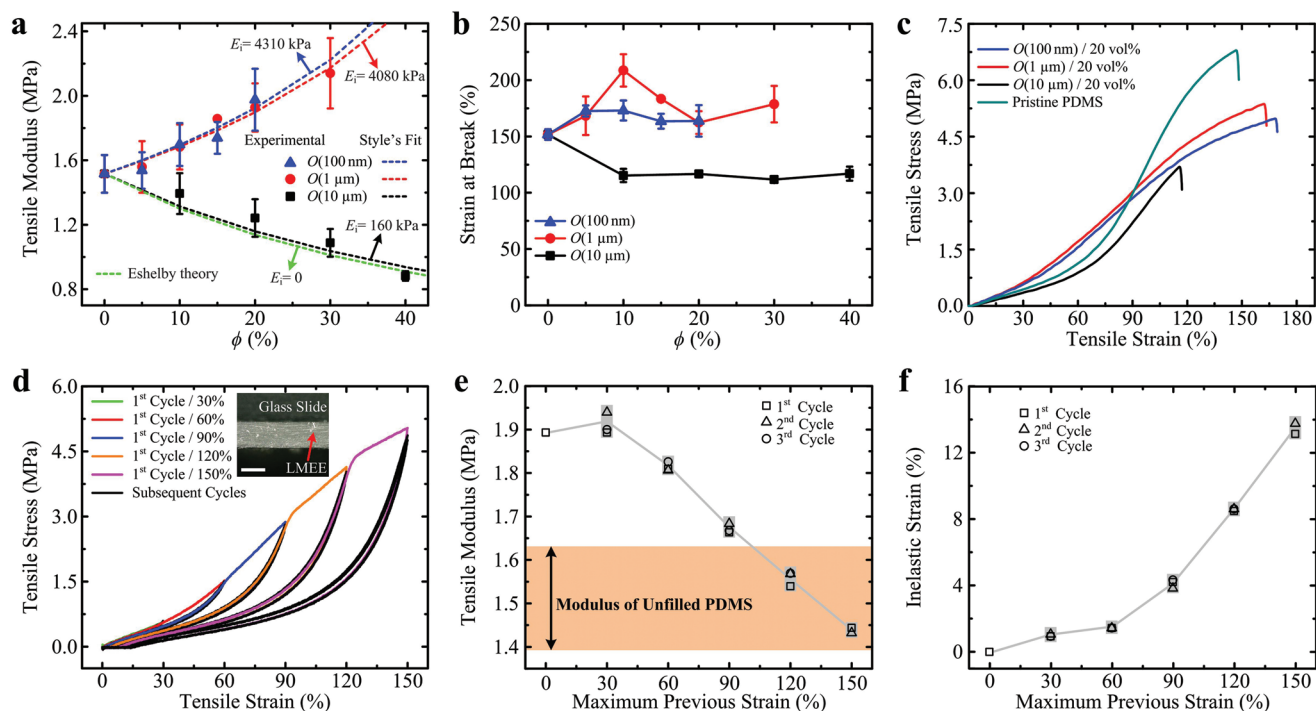


Figure 3. Mechanical properties of LM-elastomer composite. a) Tensile modulus (measured to 10% strain) as a function of LM filler content. The green dash is the prediction by Eshelby's theory^[47] and others are predictions by the Style et al. model.^[42] b) Strain at break as a function of filler content. c) Representative stress-strain curves of composites with 20 vol% of LM droplets and pristine PDMS. d-f) The LM-elastomer nanocomposite with 20 vol% LM content: d) Cyclic tensile loading of $O(100\text{ nm})$ composite with three cycles at each strain. The composite exhibits a Mullin's effect where the first loading cycle at each strain represents significant hysteresis, but negligible hysteresis during subsequent loading cycles. Inset: microscopy image of cross section of composite showing homogeneous dispersion of LM inclusion, scale bar is 200 μm . e) Normalized tensile modulus change (measured from plastic strain to +10% strain) as a function of maximum previous strain on sample. Inset: absolute tensile modulus change. f) Permanent inelastic deformation as a function of maximum previous strain.

PVDF-based dielectrics (including PVDF-HFP polymers) limits their use for applications in stretchable electronics.

In summary, the results in Figure 2 suggest that LM-elastomer nanocomposites exhibit a higher dielectric breakdown strength than microcomposites with the same LM volume fraction. This result is consistent with experimental results for composites with rigid filler^[40,41] and is also in agreement with theoretical models based on the linear dielectric breakdown electrostatics (LDBE) theory introduced by Garboczi.^[43] In particular, LM-elastomer composites with polydisperse suspensions of $O(1\text{ }\mu\text{m})$ filler exhibit the smallest degradation in dielectric breakdown strength with increasing filler content. At low loading content ($\phi = 5\%$), the composite with a more monodisperse suspension of $O(100\text{ nm})$ filler has the highest dielectric breakdown strength, although this is only slightly greater than that of the $O(1\text{ }\mu\text{m})$ composite. All three types of LM-elastomer systems exhibit a very similar response for dissipation factor and enhancement in effective relative permittivity. Lastly, a variety of polymers can be used as the matrix material for the dielectric composite.

We next study the mechanical properties of the three classes of LM-elastomer composites (Section 4, Supporting Information). First, we investigate the influence of LM inclusion size on stiffness by measuring the tensile modulus in the low-strain regime (0–10% strain). Figure 3a presents two distinct trends in the influence of volumetric fraction on stiffness—a softening trend for composites with $O(10\text{ }\mu\text{m})$ inclusions and stiffening

for composites with smaller $O(1\text{ }\mu\text{m})$ and $O(100\text{ nm})$ inclusions. With the larger inclusions, the tensile modulus decreases from 1.515 to 0.882 MPa as ϕ increases from 0 to $\phi = 40\%$. This behavior is in good agreement with the classical Eshelby theory of inclusions:^[47] $E_c = E_m/(1+5\phi/3)$ (green dash line), where E_c and E_m are the elastic modulus of composite and matrix, respectively, and the mechanical resistance of the LM inclusions is ignored. In contrast, composites with $O(1\text{ }\mu\text{m})$ and $O(100\text{ nm})$ diameter inclusions exhibit stiffening with increasing ϕ . We attribute this to the increase in relative influence of stress from the Ga_2O_3 surface oxide, droplet surface tension, and LM-polymer interphases that arise when the surface-to-volumetric ratio of the LM droplets increases. For elastomers with liquid inclusions, Style et al.^[42] had postulated that such stresses result in an equivalent elastic modulus, E_i , that is analogous to the stiffness of solid inclusions within a particle-filled elastomer composite. As in that previous study, we find that for a fixed ϕ , smaller droplets correspond to a larger E_i due to the greater interfacial area between the liquid inclusions and surrounding polymer matrix. Again assuming that the composite follows Eshelby's theory of inclusions, it follows that

$$E_c = E_m \frac{1 + \frac{2}{3} \frac{E_i}{E_m}}{\left(\frac{2}{3} - \frac{5}{3} \phi\right) \frac{E_i}{E_m} + \left(1 + \frac{5}{3} \phi\right)} \quad (2)$$

where E_i is obtained from data fitting (dash lines in Figure 3a). For the case of composites with $O(10\ \mu\text{m})$ filler, the fitted curve ($E_i = 160\ \text{kPa}$; black dashed line) is nearly indistinguishable from the classical Eshelby theory in which the stiffness of the LM inclusions is ignored (i.e., $E_i = 0$; green dashed line). However, for the LM–elastomer nanocomposites, E_i is larger than even the matrix material ($E_m = 1.515\ \text{MPa}$), which suggests that EGaIn surface effects and/or the LM–polymer interphase induce significant mechanical resistance to deformation.

The LM–elastomer composite with $O(1\ \mu\text{m})$ and $O(100\ \text{nm})$ filler can preserve similar mechanical stretchability as with the unfilled elastomer matrix, as shown in Figure 3b. However, composites with larger sized LM filler exhibit a relatively significant degradation in the strain at break, i.e., from $\approx 150\%$ to $\approx 110\%$. This reduction in stretchability agrees with the classical linear elastic fracture mechanics (LEFM) theory, which suggests that composites with larger sized filler droplets will fracture at lower stresses (and hence lower strains) than composites with smaller filler.^[43] The reduced stretchability also agrees with the theory that strain limit decreases markedly when the flaw sizes are large, i.e., bigger LM inclusions.^[48] We replot the stress–strain curves to failure for the pristine elastomer matrix and three size filler LMEE systems with $\phi = 20\%$ in Figure 3c (complete dataset in Figure S8, Supporting Information). Following an initial loading cycle, the LM–elastomer composites with different filler sizes all exhibit very low mechanical hysteresis (Figure 3d, Figure S9a,b, Supporting Information) when comparing the loading and unloading curves of subsequent cycles. The difference in the stress–strain curve for the initial loading cycle is attributed to the Mullin's effect,^[49] which can be observed each time the $O(100\ \text{nm})$ sample in Figure 3d is loaded to a new strain that exceeds the previous maximum strain. These results indicate that, for all LM inclusion sizes, the internal friction and losses from viscoelasticity or other sources of inelasticity can be neglected. We calculate the elastic modulus and permanent inelastic deformation from Figure 3d data for each loading cycle and plot these in Figure 3e,f respectively. The close agreement in the modulus and inelastic strain show that the LM–elastomer can be programmed just at the maiden mechanical deformation. As for other LM–elastomer composites,^[28] the LM–elastomer nanocomposites will be programmed to be softer and longer as the maximum previous strain applied to the sample increases. The same observation is made for composites with filler diameters of $O(1\ \mu\text{m})$ (Figure S9d, Supporting Information) and $O(10\ \mu\text{m})$ (Figure S9e; find detailed discussion in Section 4, Supporting Information). As shown in Figure 3e,f, the LM–elastomer nanocomposite can be programmed as soft as the unfilled elastomer matrix after applying adequate mechanical deformation (i.e., initial loading of $>90\%$ strain). Because of their lower resistance to mechanical deformation, softer dielectric materials have the potential to increase efficiency during conversion of mechanical work to electric energy.

Based on the results in Figure 3, we conclude that larger sized LM inclusions will soften the composite but can also lead to a reduction in strain limit. Smaller sized LM filler will stiffen the composite but can preserve the stretchability and be programmed as soft as unfilled elastomer matrix. For all composites, the addition of LM filler lowers the mechanical resistance to

stretch in the first loading cycle of a “virgin” sample. Lastly, all LM–elastomer systems exhibit very low mechanical hysteresis.

We performed two representative case studies to demonstrate how LM–elastomer nanocomposites can enhance performance in soft-matter engineering. Referring to Figure 4a, the first is an annular dielectric elastomer actuator (DEA) composed of a prestretched dielectric layer (i.e., LM–elastomer nanocomposite of 10 vol% Sylgard 184 PDMS) coated with EGaIn electrodes that are sealed with a thin polyacrylate elastomer (3M VHB tape). DEAs transform electric energy into mechanical work by coupling equal-and-opposite charge applied to the surfaces of the dielectric with an induced electrostatic pressure (so-called “Maxwell Stress”). Compared to measurements performed on a DEA sample with unfilled Sylgard 184 PDMS as the dielectric, a DEA with the LM–elastomer nanocomposite exhibits larger actuation (i.e., larger deformation) under the same electrical field ($14\ \text{kV}$; $\approx 53\ \text{kV}\ \text{mm}^{-1}$) (Figure 4b, Video S1, Supporting Information). We further examine the improved actuator performance by measuring the blocking force of the DEAs under same electric field and comparing the difference in force output (Figure 4c). The measurements are performed using the same test setup that was previously used to measure the force output of actuators powered with shape memory alloy.^[50] Three samples were tested, each sample was measured three times, and each measurement involved eleven electrical field on/off activation cycles. As necessary, the stage was readjusted between measurements to prevent the influence of initial position of DEA on blocking force (Figure 4c, left). The DEAs made of LM–elastomer nanocomposite exhibit 80% greater average blocking force than DEAs with unfilled elastomer (Figure 4c, right). This is attributed to the enhancement of Maxwell stress $\sigma_M = \epsilon_0 \epsilon_r E^2$ enabled by the larger dielectric constant ϵ_r , where ϵ_0 is the vacuum (free space) permittivity and E is the applied electric field. Figure 4d shows representative blocking force over the eleven activation cycles and suggests stable and consistent responses for both types of DEAs. We also performed cyclic actuation of LM–elastomer DEA over 3000 cycles at $0.52\ \text{Hz}$ under $9\ \text{kV}$ (Figure S12, Supporting Information). The consistent output of blocking force suggests the robustness of LM–elastomer as the compliant dielectric material for DEA.

The potential for application in energy harvesting is demonstrated with a dielectric elastomer generator (DEG). DEGs convert mechanical work to electric energy in a manner opposite to the operation of the DEA—equal-and-opposite charge on the surfaces of the dielectric undergo a change in electrostatic potential as the elastomer is deformed. The DEG, composed of a dielectric film ($\approx 320\ \mu\text{m}$) sandwiched by two EGaIn electrodes, is assembled on the acrylic holders (Figure 4e, see details in Methods). We performed constant charge conversion cycles^[51] to harvest electrical energy from mechanical work for two types of DEGs under the same condition (see details of electronics design and harvesting operation in Section 6 in the Supporting Information). The voltages across the electrodes of the two different DEGs are recorded over six energy harvesting cycles (Figure 4f, top). These curves show similar voltage history, which indicates similar capacitance change between the stretched stage and relaxed stage. The constant charge implies $Q = C_s V_s = C_i V_i$, where Q is the electric charge, C_s and V_s are the capacitance and voltage at stretched stage, respectively, and

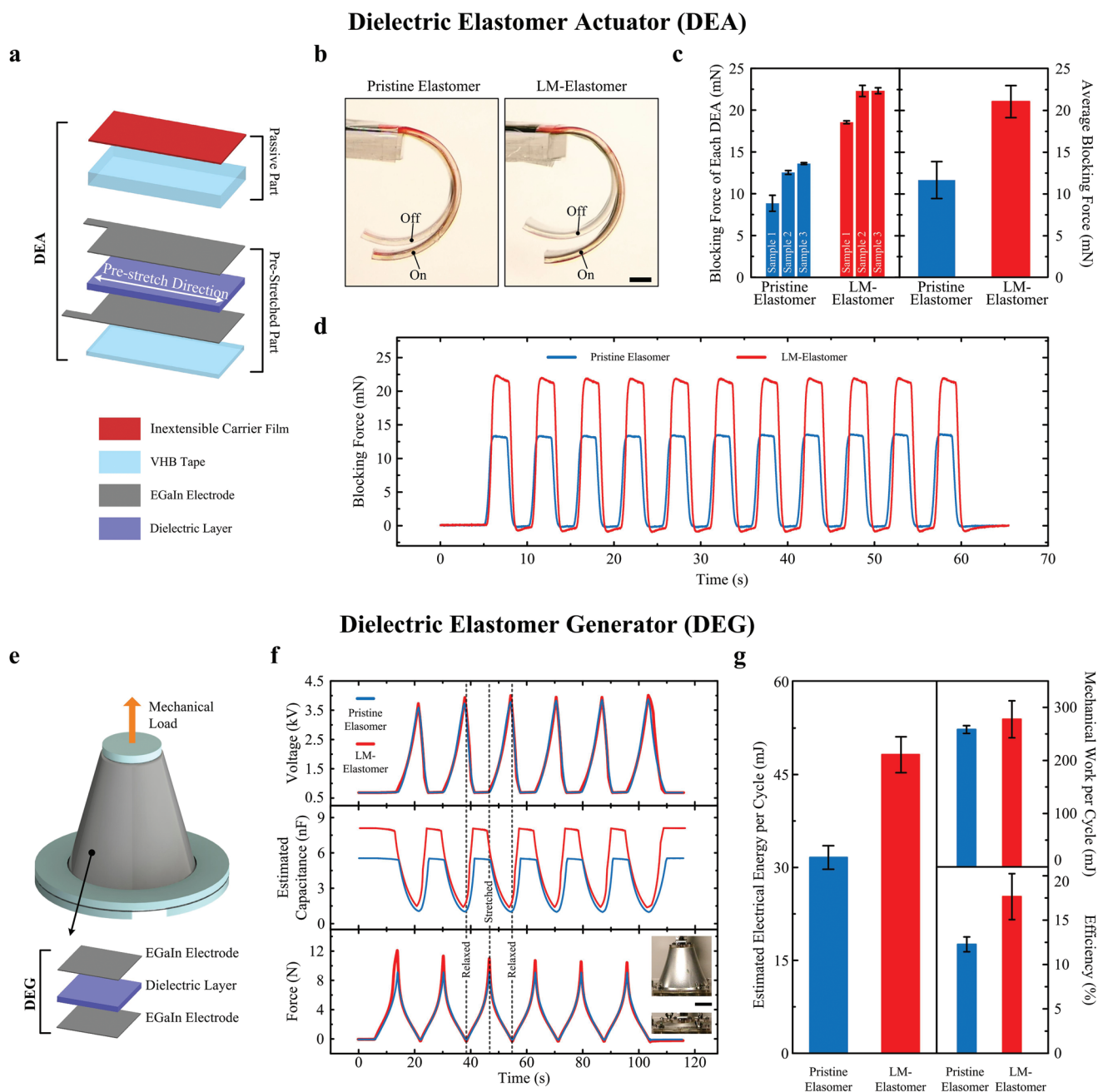


Figure 4. Demonstrations of LM-elastomer nanocomposites. a–d) Dielectric elastomer actuator (DEA) with PDMS (Sylgard 184): a) Schematic of DEA composed of prestretched dielectric layer coated with two EGaIn electrodes and thin acrylic elastomer (VHB tape), and a passive thick VHB tape with an inextensible frame on the top. b) Image of one actuation cycle of DEAs with unfilled elastomer (left) and LM-elastomer nanocomposite (right). The DEA with LM-elastomer achieves more significant actuation than unfilled elastomer. Scale bar is 5 mm. c) Blocking force of DEAs. Left: blocking force of each sample; the error bar is the standard deviation of three measurements (11 electrical field on and off cycles for each measurement) with stage-readjustment to prevent the influence of initial position of DEA on blocking force. Right: average blocking force, error bar is the standard deviation. d) Representative blocking force histories over 11 field on and off cycles. e–g) Dielectric elastomer generator (DEG) with PDMS (Ecoflex 30): e) Schematic of DEG system on stretched state. The DEG is composed of the dielectric layer sandwiched by two EGaIn electrodes. f) Top: voltage histories of DEG over 6 constant charge harvesting cycles; middle: estimated capacitance histories of DEG based on the voltage profile and constant charge; bottom: force histories from the extension of 0 (relaxed) to 80 mm (stretched). The insets are the images of the DEG with LM-elastomer on stretched stage (top) and relaxed stage (bottom). g) Left: estimated electrical energy per cycle; right-top: mechanical work per cycle; right-bottom: efficiency of electrical energy output from mechanical work input.

C_i and V_i are the current values at each time step i . We can estimate the capacitance of DEGs as a function of time (Figure 4f, middle) based on the voltage profile and C_s at the stretched

stage (LM-elastomer: 8.08 nF, unfilled elastomer: 5.54 nF, measured under 1kHz at 1V). We assume the linear dielectric property under low electric field, i.e., same capacitance between

1 and 700 V. The electrical energy (E_e) produced in one cycle from the stretched stage to relaxed stage can be estimated as

$$E_e = \frac{1}{2}(C_r V_r^2 - C_s V_s^2) = \frac{1}{2} V_r V_s C_s \left(1 - \frac{V_s}{V_r}\right) \quad (3)$$

where C_r and V_r are the capacitance and voltage at the relaxed stage, respectively. The enhancement of capacitance for the DEG with the LM–elastomer nanocomposite results in an estimated electrical energy (48.2 mJ per cycle) that is 53% greater than for a DEG with unfilled elastomer (31.6 mJ per cycle) (Figure 4g, left). Figure 4f, bottom shows the corresponding tensile load measurements as the DEGs are cycled between an extension of 0 (inset: bottom) and 80 mm (inset: top) (Video S2, Supporting Information). The LM–elastomer composite exhibits larger force compared to unfilled elastomer because the nanosized LM inclusion stiffens the composite and causes decay in force amplitude that is consistent with the observed mechanical behavior of LM–elastomer composites. In order to estimate the efficiency of the DEGs with different dielectric materials, the input mechanical work is determined by the measured force and known displacement during each cycle. Figure 4g, top right shows the average mechanical work per one cycle, i.e., mechanical work from 0 to 80 mm extension, for each DEG device, which indicates the mechanical energy input is very similar for both devices. The estimated average efficiency (ratio between electrical energy and mechanical work) of DEG devices is demonstrated in Figure 4g, bottom right. These results show that the incorporation of nanoscale LM droplets can significantly increase the efficiency of the soft energy generating transducer from 12.3% to 17.7%. The cyclical test of electrical energy harvesting for a DEG made of LM–elastomer nanocomposite was conducted at a frequency of 4.67 Hz using a home-made cyclic test system (see Video S3, Supporting Information). Figure S13 in the Supporting Information presents consistent voltage profile over 500 harvesting cycles, suggesting that LM–elastomer nanocomposites are promising for use as dielectric elastomers in high frequency DEGs.

In this work, we report a class of LM–elastomer nanocomposites that exhibit a unique combination of mechanical and dielectric properties with soft multifunctional materials never seen before. The properties of these nanocomposites, which have droplets of $O(100\text{ nm})$ diameter, are compared to composites with $O(1\text{ }\mu\text{m})$ and $O(10\text{ }\mu\text{m})$ diameter filler and a series of mechanical and electrical studies are performed in order to investigate the influence of LM filler size. LM–elastomer composites with relatively large LM inclusions, i.e., diameter of $O(10\text{ }\mu\text{m})$, exhibit a dramatic reduction in dielectric breakdown strength with increasing LM volumetric fraction ϕ . In contrast, LM–elastomer composites with $O(1\text{ }\mu\text{m})$ - and $O(100\text{ nm})$ -sized inclusions exhibit a more steady linear decrease in E_b , with the $O(1\text{ }\mu\text{m})$ composites showing a slightly lower reduction possibly due to its greater polydispersity (i.e., combination of nano- and micro-sized droplets). The effective dielectric constant of the LM–elastomer composites generally follows the same trends predicted by effective medium theory (Bruggeman formulation), although a fitting is required to correct for the poor polarizability of the LM–polymer interface. In addition to their reduced influence on dielectric breakdown strength, smaller

LM inclusion are also observed to preserve the strain limit (i.e., stretchability) of the polymer matrix, which is consistent with principles in linear elastic fracture mechanics.^[43,48] Moreover, as predicted by Style et al.,^[42] smaller LM inclusions also lead to mechanical stiffening, although the composite remains soft and highly deformable compared to other dielectric polymer composites. Lastly, although a Mullin's effect is observed for the initial loading of a virgin sample, the LM–elastomer composites generally exhibit highly elastic behavior with negligible mechanical hysteresis. This unique combination of enhanced electric permittivity, controlled dielectric breakdown strength, and rubber-like mechanical properties enable LM–elastomer nanocomposites to have transformative impact in soft materials actuation, energy storage, and energy harvesting.

Experimental Section

LM–Elastomer Composites Preparation: For LM–elastomer composites with diameters of $O(100\text{ nm})$ and $O(1\text{ }\mu\text{m})$, first bulk EGaIn are broken down into nanoscale droplets by ultrasonication in methylisobutylketone (MIBK) without any surfactant. The EGaIn droplets are stable due to the thin solid Ga_2O_3 skin. Next, the solution was placed in a glass vial and centrifuged in order to enable the EGaIn droplets to settle and the solvent to be decanted. The uncured elastomer matrix was then poured into the vial and mixed with the droplets using a planetary shear mixer. Although the EGaIn solution was decanted, a small amount of solvent remained trapped between droplets. This solvent acted as a “lubricant” that separated the droplets and prevented their aggregation. During mixing with the uncured elastomer, the nanodroplets were dragged apart by viscous shear forces and homogeneously dispersed within the matrix. Compared to probe sonication or magnetic stirring for nanodroplets dispersion, planetary mixing was capable of handling highly viscous polymers that provide adequate mechanical resistance to prevent sedimentation of the more dense LM droplets. For composites with $O(10\text{ }\mu\text{m})$ droplets, the ultrasonication step was skipped and bulk EGaIn and the liquid elastomer were mixed using the planetary mixer. The details of fabrication process can be found in Section 1 in the Supporting Information.

Nano-CT Scan: The morphology of the LM–elastomer composites was analyzed with a nanoscale X-ray computational tomography (nano-CT) instrument (UltraXRM L200, Xradia, Inc. Pleasanton, CA, USA). The details of setting can be found in Section 1 in the Supporting Information.

Dielectric Properties Measurement: A benchtop LCR meter (889B; BK Precision) was used to measure the capacitance and dissipation factor. Then the corresponding effective dielectric constant was back-calculated. After this, the dielectric breakdown strength was measured using a high voltage power supply (PS 365, Stanford Research Systems) to supply DC voltage with the ramp of 500 V s^{-1} , except for composites with $O(10\text{ }\mu\text{m})$ LM inclusion, in which case 5 V s^{-1} was used. The dielectric breakdown strength was done using a two-parameter Weibull statistical model described by the cumulative distribution function $P(E) = 1 - 1/\exp((E_b/\alpha)^\beta)$, where P is the probability of electric failure, E_b is the experimental breakdown field, the scale parameter α (Weibull E_b) represents the field strength for 63% probability for the sample to electrical breakdown, and β is the shape parameter corresponding to the scatter of experimental data. At least 15 data points per sample were collected to extract the Weibull breakdown strength. The details of sample preparation can be found in Section 1 in the Supporting Information.

Mechanical Properties Measurement: Samples were tested on a materials testing system (Instron 5969, Illinois Tool Works Inc) with a 50 N load cell and extension rate of 20 mm s^{-1} . The details of sample preparation can be found in Section 1 in the Supporting Information.

DEA Fabrication and Characterization: The DEAs were actuated at 14 kV ($\approx 53\text{ kV mm}^{-1}$) for film the actuation video and blocking force

measurement. A previously reported method was followed^[50] for testing the blocking force of bending actuators with a material testing system and 10 N load cell. The details of sample preparation are presented in Section 1 in the Supporting Information.

DEG Fabrication and Characterization: The details of the DEG electrical energy circuit system and characterization process are presented in Section 6 in the Supporting Information. The details of sample preparation can be found in Section 1 in the Supporting Information.

Supporting Information

Supporting Information is available from the Wiley Online Library or from the author.

Acknowledgements

The authors thank Keene Chin (Robotics Institute; Carnegie Mellon University) for particles size detection from SEM images. This work was supported by support by the National Science Foundation CMMI program (Civil, Mechanical, and Manufacturing Innovation; Dr. Mary M. Toney; Award 1635824) and AFOSR Multidisciplinary University Research Initiative (FA9550-18-1-0566; Program Manager: K. Goretta).

Conflict of Interest

The authors declare no conflict of interest.

Keywords

dielectric elastomer actuators, dielectric elastomer generators, liquid-metal nanodroplets, liquid-metal–elastomer nanocomposites, stretchable dielectric materials

Received: January 27, 2019

Revised: March 20, 2019

Published online:

- [1] K. K. Kim, S. Hong, H. M. Cho, J. Lee, Y. D. Suh, J. Ham, S. H. Ko, *Nano Lett.* **2015**, *15*, 5240.
- [2] N. Matsuhisa, D. Inoue, P. Zalar, H. Jin, Y. Matsuba, A. Itoh, T. Yokota, D. Hashizume, T. Someya, *Nat. Mater.* **2017**, *16*, 834.
- [3] J. Wang, G. Cai, S. Li, D. Gao, J. Xiong, P. S. Lee, *Adv. Mater.* **2018**, *30*, 1706157.
- [4] Y. Z. Wu, Y. W. Liu, Y. L. Zhou, Q. K. Man, C. Hu, W. Asghar, F. L. Li, Z. Yu, J. Shang, G. Liu, M. Y. Liao, R. W. Li, *Sci. Rob.* **2018**, *3*, eaat0429.
- [5] C. Larson, B. Peele, S. Li, S. Robinson, M. Totaro, L. Beccai, B. Mazzolai, R. Shepherd, *Science* **2016**, *351*, 1071.
- [6] Z. F. Liu, S. Fang, F. A. Moura, J. N. Ding, N. Jiang, J. Di, M. Zhang, X. Lep  r  , D. S. Galv  o, C. S. Haines, N. Y. Yuan, S. G. Yin, D. W. Lee, R. Wang, H. Y. Wang, W. Lv, C. Dong, R. C. Zhang, M. J. Chen, Q. Yin, Y. T. Chong, R. Zhang, X. Wang, M. D. Lima, R. Ovalle-Robles, D. Qian, H. Lu, R. H. Baughman, *Science* **2015**, *349*, 400.
- [7] G. Z. Lum, Z. Ye, X. Dong, H. Marvi, O. Erin, W. Hu, M. Sitti, *Proc. Natl. Acad. Sci. USA* **2016**, *113*, E6007.
- [8] C. Keplinger, J. Y. Sun, C. C. Foo, P. Rothmund, G. M. Whitesides, Z. Suo, *Science* **2013**, *341*, 984.
- [9] Q. Li, L. Chen, M. R. Gadinski, S. Zhang, G. Zhang, H. U. Li, E. Iagodkine, A. Haque, L.-Q. Chen, T. N. Jackson, Q. Wang, *Nature* **2015**, *523*, 576.
- [10] Q. Li, G. Zhang, F. Liu, K. Han, M. R. Gadinski, C. Xiong, Q. Wang, *Energy Environ. Sci.* **2015**, *8*, 922.
- [11] D. J. Lipomi, Z. A. Bao, *Energy Environ. Sci.* **2011**, *4*, 3314.
- [12] Y. Xie, Y. Yu, Y. Feng, W. Jiang, Z. Zhang, *ACS Appl. Mater. Interfaces* **2017**, *9*, 2995.
- [13] X. Zhang, Y. Shen, B. Xu, Q. Zhang, L. Gu, J. Jiang, J. Ma, Y. Lin, C. W. Nan, *Adv. Mater.* **2016**, *28*, 2055.
- [14] C. C. Kim, H. H. Lee, K. H. Oh, J. Y. Sun, *Science* **2016**, *353*, 682.
- [15] D. J. Lipomi, M. Vosgueritchian, B. C. K. Tee, S. L. Hellstrom, J. A. Lee, C. H. Fox, Z. Bao, *Nat. Nanotechnol.* **2011**, *6*, 788.
- [16] D. Son, J. Kang, O. Vardoulis, Y. Kim, N. Matsuhisa, J. Y. Oh, J. W. F. To, J. Mun, T. Katsumata, Y. Liu, A. F. McGuire, M. Krasov, F. Molina-Lopez, J. Ham, U. Kraft, Y. Lee, Y. Yun, J. B. H. Tok, Z. Bao, *Nat. Nanotechnol.* **2018**, *13*, 1057.
- [17] J. Y. Sun, C. Keplinger, G. M. Whitesides, Z. Suo, *Adv. Mater.* **2014**, *26*, 7608.
- [18] L. Hines, K. Petersen, G. Z. Lum, M. Sitti, *Adv. Mater.* **2017**, *29*, 1603483.
- [19] W. Hu, G. Z. Lum, M. Mastrangeli, M. Sitti, *Nature* **2018**, *554*, 81.
- [20] J. Park, S. Choi, A. H. Janardhan, S.-Y. Lee, S. Raut, J. Soares, K. Shin, S. Yang, C. Lee, K. W. Kang, H. R. Cho, S. J. Kim, P. Seo, W. Hyun, S. Jung, H. J. Lee, N. Lee, S. H. Choi, M. Sacks, N. Lu, M. E. Josephson, T. Hyeon, D. H. Kim, H. J. Hwang, *Sci. Transl. Med.* **2016**, *8*, 344ra86.
- [21] S. Choi, S. I. Han, D. Jung, H. J. Hwang, C. Lim, S. Bae, O. K. Park, C. M. Tschabrunn, M. Lee, S. Y. Bae, J. W. Yu, J. H. Ryu, S.-W. Lee, K. Park, P. M. Kang, W. B. Lee, R. Nezafat, T. Hyeon, D.-H. Kim, *Nat. Nanotechnol.* **2018**, *13*, 1048.
- [22] S. H. Kim, S. Jung, I. S. Yoon, C. Lee, Y. Oh, J. M. Hong, *Adv. Mater.* **2018**, *30*, 1800109.
- [23] K. Y. Chun, Y. Oh, J. Rho, J. H. Ahn, Y. J. Kim, H. R. Choi, S. Baik, *Nat. Nanotechnol.* **2010**, *5*, 853.
- [24] S. Lee, S. Shin, S. Lee, J. Seo, J. Lee, S. Son, H. J. Cho, H. Algadi, S. Al-Sayari, D. E. Kim, T. Lee, *Adv. Funct. Mater.* **2015**, *25*, 3114.
- [25] C. Wang, C. Wang, Z. Huang, S. Xu, *Adv. Mater.* **2018**, *30*, 1801368.
- [26] G. Wang, X. Huang, P. Jiang, *ACS Appl. Mater. Interfaces* **2015**, *7*, 18017.
- [27] M. D. Bartlett, A. Fassler, N. Kazem, E. J. Markvicka, P. Mandal, C. Majidi, *Adv. Mater.* **2016**, *28*, 3726.
- [28] M. D. Bartlett, N. Kazem, M. J. Powell-Palm, X. Huang, W. Sun, J. A. Malen, C. Majidi, *Proc. Natl. Acad. Sci. U.S.A.* **2017**, *114*, 2143.
- [29] R. Tutika, S. H. Zhou, R. E. Napolitano, M. D. Bartlett, *Adv. Funct. Mater.* **2018**, *28*, 1804336.
- [30] M. I. Ralphs, N. Kemme, P. B. Vartak, E. Joseph, S. Tipnis, S. Turnage, K. N. Solanki, R. Y. Wang, K. Rykaczewski, *ACS Appl. Mater. Interfaces* **2018**, *10*, 2083.
- [31] S. H. Jeong, S. Chen, J. Huo, E. K. Gamstedt, J. Liu, S.-L. Zhang, Z.-B. Zhang, K. Hjort, Z. Wu, *Sci. Rep.* **2016**, *5*, 18257.
- [32] G. Gallone, F. Carpi, D. De Rossi, G. Levita, A. Marchetti, *Mater. Sci. Eng., C* **2007**, *27*, 110.
- [33] J. Cho, M. S. Joshi, C. T. Sun, *Compos. Sci. Technol.* **2006**, *66*, 1941.
- [34] A. Koh, J. Sietins, G. Slipper, R. Mrozek, *J. Mater. Res.* **2018**, *33*, 2443.
- [35] N. Kazem, M. D. Bartlett, C. Majidi, *Adv. Mater.* **2018**, *30*, 1706594.
- [36] A. Fassler, C. Majidi, *Adv. Mater.* **2015**, *27*, 1928.
- [37] Z. Yu, J. Shang, X. Niu, Y. Liu, G. Liu, P. Dhanapal, Y. Zheng, H. Yang, Y. Wu, Y. Zhou, Y. Wang, D. Tang, R.-W. Li, *Adv. Electron. Mater.* **2018**, *4*, 1800137.
- [38] E. J. Markvicka, M. D. Bartlett, X. Huang, C. Majidi, *Nat. Mater.* **2018**, *17*, 618.
- [39] N. Kazem, T. Hellebrekers, C. Majidi, *Adv. Mater.* **2017**, *29*, 1605985.
- [40] J. K. Nelson, C. F. John, *Nanotechnology* **2004**, *15*, 586.
- [41] M. Roy, J. K. Nelson, R. K. MacCrone, L. S. Schadler, C. W. Reed, R. Keefe, *IEEE Trans. Dielectr. Electr. Insul.* **2005**, *12*, 629.
- [42] R. W. Style, R. Boltyskiy, B. Allen, K. E. Jensen, H. P. Foote, J. S. Wettlaufer, E. R. Dufresne, *Nat. Phys.* **2015**, *11*, 82.
- [43] E. J. Garboczi, *Phys. Rev. B* **1988**, *38*, 9005.

- [44] C. W. Nan, R. Birringer, D. R. Clarke, H. Gleiter, *J. Appl. Phys.* **1997**, *81*, 6692.
- [45] J. J. Marcinko, A. A. Parker, Y. T. Shieh, W. M. Ritchey, *J. Appl. Polym. Sci.* **1992**, *45*, 391.
- [46] A. C. Jayasuriya, S. Tasaka, T. Shouko, N. Inagaki, *J. Appl. Phys.* **1996**, *80*, 362.
- [47] J. D. Eshelby, *Proc. R. Soc. A* **1957**, *241*, 376.
- [48] C. Chen, Z. Wang, Z. Suo, *Extreme Mech. Lett.* **2017**, *10*, 50.
- [49] L. Mullins, *Rubber Chem. Technol.* **1969**, *42*, 339.
- [50] X. Huang, K. Kumar, M. K. Jawed, A. Mohammadi Nasab, Z. Ye, W. Shan, C. Majidi, *Adv. Mater. Technol.* **2019**, 1800540.
- [51] S. Chiba, M. Waki, T. Wada, Y. Hirakawa, K. Masuda, T. Ikoma, *Appl. Energy* **2013**, *104*, 497.